Research Article

Shiraz University

Mechanical analysis of cluster-grain separator device of a new head of paddy harvesting machine

H. Azimi-Nejadian*[1], T. Tavakoli-Hashjin[2], M. A. Nematollahi[1], S. H. Karparvarfard[1]

Department of Biosystems Engineering, College of Agriculture, Shiraz University, Shiraz, I. R. Iran
Department of Biosystems Engineering, College of Agriculture, Tarbiat Modares University, Tehran, I. R. Iran

* Corresponding Author: h.aziminejadian@shirazu.ac.ir

ABSTRACT- This paper presents stress and strain analysis of outer shaft shoulder (OSS) and inner shaft shoulder (ISS) of a new paddy harvesting head (PHH) using finite element method (FEM). Snapping grain unit is a part of this head, with OSS and ISS as its members. The analysis was performed using the ABAQUS software with Dynamics Explicit Solution Method. Eight-node block and four-node tetrahedral elements were used to mesh the parts of the head. After the analyses, the stress and strain curves, and their maximum values were estimated for various parts. Analytical method was used to verify the FEM results and to calculate the factor of safety (FS) of the OSS and ISS components and also to estimate the number of cycles to failure of each component. The maximum amount of force applied to each tooth of shoulder was 4.29 Nmm^{-1}. The maximum stress in both shoulders was obtained as 44.43 MPa. Other results showed, fatigue factors of safety for all components were less than their relevant yield factor of safety. Therefore, the fatigue in components would occur first. The study showed the predicted life for OSS and ISS components is more than 10^6 cycles, thus the components have an infinite-life. A fitted regression line to the data showed that the calculated stresses from analytical method lie within bounds of ± 7.89 % of the predicted values with a coefficient of determination of 0.98. Hence, it could be concluded that there is a good agreement between the analytical and FEM results.

Nomenclature

Symbols			
α, β	Constant coefficients	S_{ut}	Ultimate stress (N m^{-2})
c	Perpendicular distance to the neutral axis (m)	s_y	Yield stress (N m^{-2})
f	Fatigue strength fraction coefficients	t	Thickness (width) (m)
I	Second moment of area about the neutral axis (m^4)	V	Total shear force (N)
k_a	Surface condition modification factor	σ	Bending stress (N m^{-2})
K_b	Size modification factor	σ_a	Amplitude component of bending stress (N m^{-2})
K_c	Load modification factor	σ_m	Midrange component of bending stress (N m^{-2})
K_d	Temperature modification factor	σ_{max}	Maximum bending stress (N m^{-2})
K_e	Reliability factor	σ_{min}	Minimum bending stress (N m^{-2})
K_f	Miscellaneous-effects modification factor	$\sigma_a{}'$, $\sigma_m{}'$	Von Mises components stress (N m^{-2}),
M	Moment about the neutral axis (N.m)	σ_{Von}	Von Misses stress N m^{-2})
N	Cycles to failure (cycle)	σ_x, σ_y, σ_z	Stress in x, y and z direction, respectively (N m^{-2}).
N_f	Fatigue factor of safety	τ	Shear stress (N m^{-2})
N_y	Yield factor of safety	τ_a	Amplitude component of shear stress (N m^{-2})
S_e	Endurance limit at the critical location of a machine part (N m^{-2})	τ_m	Midrange component of shear stress (N m^{-2})
S_f	Fatigue strength (N m^{-2})	τ_{max}	Maximum shear stress (N m^{-2})
Q	First moment of area (m^3)	τ_{min}	Minimum shear stress (N m^{-2})
S_e	Rotary-beam test specimen endurance limit (N m^{-2})	τ_{xy}, τ_{yz}, τ_{xz}	Shear stress in x-y, y-z and x-z plans respectively (N m^{-2}).

INTRODUCTION

Rice is the principal main food for more than a third of the world's population and the need for it has increased in Iran in recent years (Horgan et al., 2016; Motevali et al., 2019). In rice cultivation, harvesting is the most important operation. It is harvested either by manual labor in traditional method or by rice combines (Elsoragaby et al., 2019). Traditional paddy harvesting is usually delayed due to labor scarcity which results in losing grain due to over maturity, therefore, the low performance of traditional harvesting process has forced farmers to shift into mechanical grain harvesting (Chandrajith et al., 2016). Many studies have been conducted to optimize the performance of agricultural machinery .This subject has attracted the attention of many researchers. Nowadays, analyzing the mechanical behavior of the systems in respect of the applied forces, stress and strain distributions, deformations, optimization of the performance of components and structures is more efficient and faster by computer-aided design techniques (Jahanbakhshi et al., 2017; Jahanbakhshi & Heidarbeigi, 2019). The finite element method (FEM) is an efficient and accurate numerical technique to perform the stress–strain and deformation analysis of mechanical parts and to identify the critical points before production of the first prototype (Beni et al., 2013; Seyedabadi, 2015; Fadaei and Mokhtari, 2015; Fu et al., 2016; Heintze et al, 2018; Ucgul et al., 2018; Ushio et al., 2019). The ABAQUS software is one of the most commonly used softwares for finite element analysis and computer-aided engineering tasks, which is widely used to model the farm machinery (Muntakim et al., 2016; Gao, 2019; Azimi-Nejadian et al., 2019). In this respect, a research was conducted to dynamic analysis and reliability design of round baler feeding device for rice straw harvest. The FEM simulations at different values of displacement and throughput was carried out and results were used to improve reliability, safety factors for the feeding devices (Zhao et al., 2018). The FEM was used for both static and fatigue analysis of a low-cost mini combine harvester chassis and hitch design by Abdulkarim et al. (2017). The stresses, strain and displacements on the chassis were determined and the factors of safety were found to be 2.48 and 2.80 for chassis and hitch, respectively. Then the FEM results were compared to experimental data and the results showed that the FEM results are more reliable. The frontal combine harvester axle analyzed and designed a using FEM and experimental methods. The FEM results were verified with the experimentally method and this method was in good agreement with experimental data. Results obtained by FEM showed that the proposed model was suitable to install on the modified combine (Khanali et al., 2010). It was shown that the success and reliability of the results in a numerical analysis were heavily dependent upon work material flow stress, friction parameters between the tool and work material interfaces, the fracture criterion, and the thermal parameters (Shaw, 2005; Umbrello, 2008; denguir et all, 2017). Therefore, the correct selection of these parameters plays an important role in the reasonable estimation of the goal. Many researchers simulated the behavior of the bolt–nut assembly using three-dimensional solid elements in order to be closer to reality (Yorgun et al., 2004; McCarthy et al., 2005; Elsawaf and Hassan, 2018). In some studies, (Bursi and Jaspart, 1998; Kim et al., 2007; Reid and Hiser, 2005), the bolt shank as well as bolt head were modelled using beam elements. Shahani et al. (2015) estimated the fatigue life of the bolt connecting two flanges using ABAQUS software. The fatigue properties of the bolt were measured in the laboratory according to ISO 3800 standard, while the amount of stress applied to the bolt was calculated using the FEM. Finally, given the nominal bolt stress calculated by the software and using the fatigue properties from experiments, the fatigue life of the bolt was estimated. It was reported that when members of a system were in contact together, explicit finite element should be used to analyze and penalty contact algorithm to describe mechanical interaction between the members (Fu and Chui, 2014; Jain et al., 2018).

In this study a new head of paddy harvesting machine is introduced. The ISS and OSS parts are two components of the snapping grain unit. To design and fabricate the snapping grain unit, it is needed to model and analyze the mentioned system. The main objective of the analysis was to find the critical sections of the snapping grain unit and obtain the maximum stress and strain in the critical sections to prevent the failure by the applied external loadings. In addition, the factor of safety was determined by the Von-Mises criteria to ensure the parts work safety. For this purpose, the stress and strain analysis of the head OSS and ISS head were performed using the FEM. This information can be used to optimize the head.

MATERIALS AND METHODS

Introducing the Paddy Harvesting Head (PHH)

This head was designed for direct harvest of paddy grains from its spike (Fig. 1). This PHH can be attached in front of a tractor. It consists of gatherer point unit, snapping grain unit, power production and transmission, shoulders opening and closing units and the frame. As the tractor moves through the field, the gatherer points are positions between the rows of rice plants. Snapping shoulder grab the paddy stalks and pull them rapidly down between the shoulder teeth. When a spike paddy reaches the snapping shoulder, the paddy grain is prevented from going through because of the narrow opening of shoulder teeth. The snapping shoulder continues to pull on the stalk and snap the paddy grain free of the spike (Fig. 2).

Gatherer Point Unit

Rice seedlings are usually transplanted by rice-transplanters in regular rows. This PHH was designed for harvesting crops that planted on rows. Therefore, gatherer point arranges the rice plants in a row. This action helps the snapping grain unit to do its duty better

34

Snapping Grain Unit

Paddy grains are connected to a spike with a thin thread (pedicel) and they have no cover. Therefore, they can be separated from the spike with a small force (Fig. 3b). This rice spike property was used to design the snapping grain unit. This unit is consisted of OSS, ISS, outer shaft (OS), and inner shaft (IS). The OSS and ISS were attached to their shafts. The OS has only rotational movement but the IS has both rotational and reciprocating movements. Thus, ISS has both rotational and reciprocate movements because it is attached to the IS. The IS's reciprocating movement cause a group of shoulders to be placed in the closing position and the other group placed at the opening position. When the shoulders are in closing position, they snap the grains from the cluster as shown in Fig. 2(d).

Power and Transmission Units

A hydraulic motor was used to generate the power required for the head operation. This hydraulic motor is driven by the tractor hydraulic system. The power is transmitted by pulley and belt to the OS of the snapping grain unit (Fig. 2c).

Shoulders Opening and Closing Units

As mentioned before, ISS has the rotational and reciprocating motions. As the ISS is coupled to the OSS, these two shafts turn together at the same rotational speed. As the ISS needs to exert a reciprocating movement to open and close the shoulders, this reciprocating movement is generated by a cam (Fig. 2a).

Measurement of the required force to snap the paddy

A simple tool was used to measure the tensile force required for snapping the paddy grains from the cluster. This tool is composed of a shoulder and a rod (Fig. 3a). The rod is connected to the Universal Testing Machine (Instron) and the paddy clusters are placed between the shoulder teeth (Fig. 3b). By raising the upper jaw of the unit, the paddy grains are snapped from the cluster by shoulder teeth. The experiments were performed at five levels of jaw velocity including 100, 200, 300, 400, and 500 mm min^{-1}, and each experiment replicated three times.

The Mechanical Analysis of Parts

The OSS Stress and Strain Analysis

The OSS components and their dimensions are shown in Fig. 4(a). In this figure, part 4 is the OS to which the shoulder components are attached. Part a is the shoulder and parts b and c are welded to the shoulder and OS, respectively. These two parts join the shoulder to the OS (Fig. 4a).

The maximum rotational speed of the shaft shoulders was considered as 200 RPM (Azimi Nejadian, 2016). Therefore, the analysis should be done at this angular velocity. Shoulder analysis in a complete cycle is time-consuming, so only 45 degrees of the shoulder rotation was analyzed. This is the most critical period of the shoulder rotation and the loads were applied to shoulder only in this period.
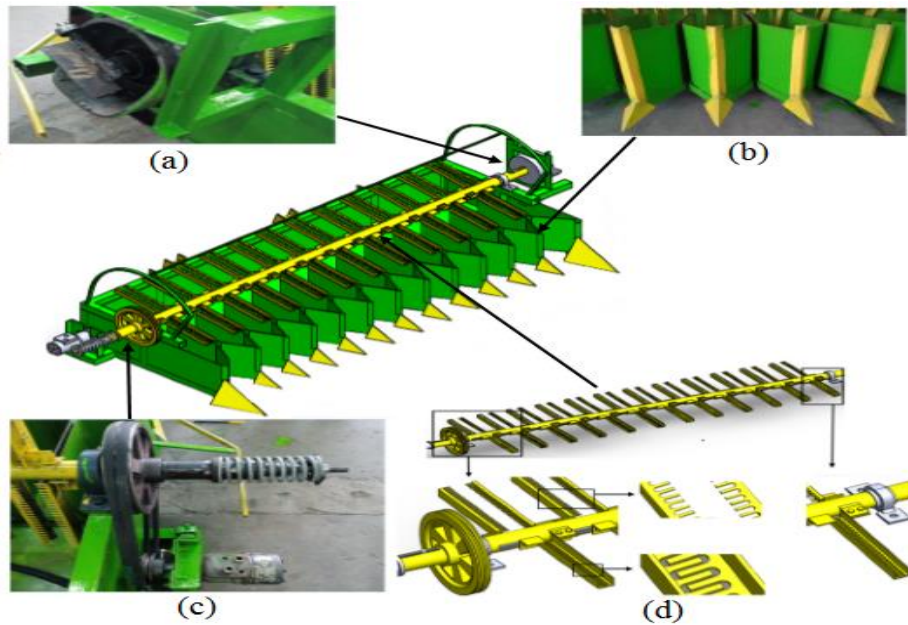

Fig.1. Paddy harvesting head.

Fig.2. Paddy harvesting head and its components; (a) Shoulders opening and closing unit; (b) Gatherer point unit; (c) Power production and transmission system; (d) Snapping grain unit.

<div style="text-align:center">(a)   (b)</div>

Fig.3. (a) A simple tool was used to measuring tensile force; (b) Display the snapping of the grains paddy from the cluster by shoulder.

The dynamic explicit method for the dynamic analysis is better to be used for structures that have been composed of several parts which are in contact with each other (Harewood and Mchugh, 2007; Tanlak et al., 2011). Thus, in this study, analyses were done using explicit dynamics. Two time steps were considered for the analysis. In the first step, shoulder speed reaches from zero to 200 RPM and the load is applied in the second step in which the rotational speed is constant. Shoulder components were made from St37 steel. The mechanical properties of St37 steel required in the analysis are listed in Table 1. To assemble the OSS components, two (M8× 1.25) 5.8 grade bolts were used (Shigley, 2011).

After modelling the shoulder and selecting its material properties, the grain snapping force (see below.) was applied on the shoulder teeth. In order to calculate the maximum force exerted to each tooth, with regard to the dimensions of the rice stem and its smallest cross section, the maximum number of clusters that could place in the space between the shoulders was estimated. Therefore, the number of clusters in the space between the two shoulders was estimated and the force necessary to snap the seeds from the spike has been already measured (Azimi nejadian et al., 2016). Finally, according to the length of each tooth (Fig. 4c), the maximum amount of force exerted to each tooth of shoulder was obtained as 4.29 Nmm^{-1}. The purpose of the analysis of this part of the head (OSS) was to determine the distribution of stress and strain in parts a, b, and c (Fig. 4a). It should be noted that part d is not subject to analysis as it was considered as a rigid body. The required parameters for the analysis by the explicit dynamic method (Azimi Nejadian, 2016) are listed in Table 2.

The interactions between the bolt shank and the holes of part b and c; bolt nut and part b; and surfaces of part b and part c were modeled using surface to surface contacts. In this analysis the eight-node block elements were used to mesh the OSS and ISS components. Considering computational efficiency, the mesh density is an important factor in the analysis. To achieve accurate results, the appropriate elements type and their dimensions must be properly selected. Simulations were launched with the large elements, then elements were refined until the results did not significantly change. For meshing of shoulder components, the eight-node block element (C3D8) was used and it was discretized into 158211 elements (Fig. 4d).
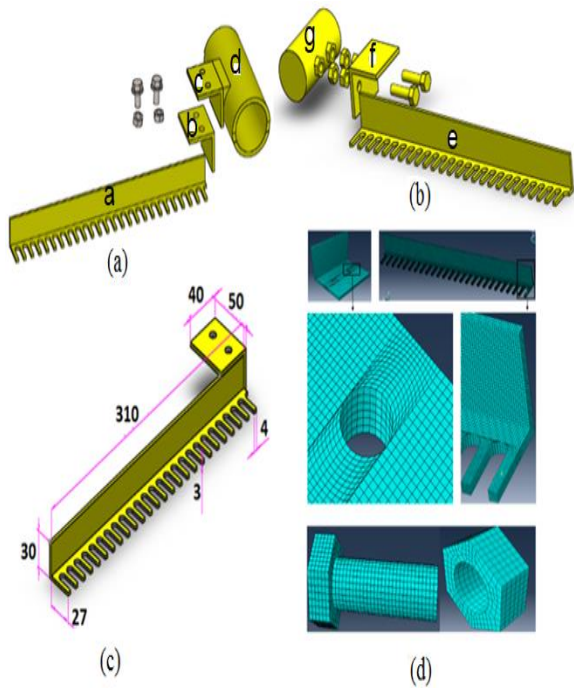
Fig. 4. (a) OSS components; (b) ISS components; (c) Shoulder dimension in millimeter; (d) Shoulder components mesh.

Table 1. Parts mechanical properties (Shigley, 2011; Soltani and Tabatabaei Mirhosseini, 2013).

Shoulder	Bolts and Nuts	Property
Young's modulus (N/m^2)	2×10	2.1×10^9
Poisson's ratio	0.3	0.3
Density (Kg/m^3)	7850	7850
Yield stress (Mpa)	420	240
Ultimate stress (Mpa)	520	370

Table 2. OSS loading and boundary conditions (Azimi Nejadian, 2016).

Step number	Time (s)	The amount of rotation (degree)	Rotational speed (Radians/s)	linear force (N/mm)
1	0.0125	15	20.92	0
2	0.025	30	20.92	4.29

The ISS Analysis

The ISS components' geometry are shown in Fig. 4(b). Part g is the shoulder driver (IS) and was considered as a rigid body, boundary conditions such as rotational speed and the degree of freedom were defined on this part (Table 2). The force applied on both ISS and OSS is equal and consequently the distribution of stress and strain in part e of Fig. 6 is similar to part a of Fig. 4. In order to reduce the analysis time, part a was considered as a rigid body. Solving steps, material properties, loads, boundary conditions, and components meshing of ISS are similar to those mentioned in the previous section. The interaction between the bolt shank and the inner

surface of the nut, surfaces of part e and part f, surface of nuts and part g, and surfaces of nuts and bolt head with part f were modeled in the software.

Fatigue Analysis

The purpose of this section was to calculate the components factors of safety (FS) and estimate the number of cycles to failure of components. Depending on the desired use for a product, individual components need to be assessed as accurately as possible for expected conditions. Factor of safety is a term to describe the load carrying capability of a system beyond the expected or actual loads. The Oss and ISS are subjected to various components of stress and cyclic loading. The shoulder was modeled as a beam. Therefore, the shear and bending stresses for this component can be written as below (Shigley, 2011).

$$\sigma = Mc/I \qquad (1)$$
$$\tau = VQ/It \qquad (2)$$

Fluctuating stresses in components usually take the form of a sinusoidal pattern. Thus, the amplitude and midrange components of shear and normal stresses are as follows (Shigley, 2011).

$$\sigma_a = \sigma_{max} - \sigma_{min}/2 \qquad (3)$$
$$\sigma_m = \sigma_{max} + \sigma_{min}/2 \qquad (4)$$
$$\tau_a = \tau_{max} - \tau_{min}/2 \qquad (5)$$
$$\tau_m = \tau_{max} + \tau_{min}/2 \qquad (6)$$

Finally, the modified Goodman failure criteria was used to calculate the factor of safety. Therefore, the equations to calculate the FS are as follows (Shigley, 2011).

$$S_e' = 0.504\ S_{ut} \qquad (7)$$
$$S_e = k_a k_b k_c k_d k_e k_f S_e' \qquad (8)$$
$$\sigma_a' = (\sigma_a^2 + 3\tau_a^2)^{\frac{1}{2}} \qquad (9)$$
$$\sigma_m' = (\sigma_m^2 + 3\tau_m^2)^{\frac{1}{2}} \qquad (10)$$
$$1/n_f = \sigma_a'/S_e + \sigma_m'/S_{ut} \qquad (11)$$
$$n_y = s_y/\sigma_a' + \sigma_m' \qquad (12)$$

Also, the modified Goodman failure criteria was used to estimate the number of cycles to failure of components. Therefore, the equations to estimate the number of cycles to failure are as follows (Shigley, 2011).

$$S_f = \sigma_a'/1 - \sigma_m'/S_{ut} \qquad (13)$$
$$N = (S_F/\alpha)^{1/\beta} \qquad (14)$$
$$\alpha = (fS_{ut})^2/S_e \qquad (15)$$
$$\beta = -(1/3)\log(fS_{ut}/S_e) \qquad (16)$$

RESULTS AND DISCUSSION

Grain Snapping Force

The force required to snap the grain paddy from the spike, over the displacement of shoulder was plotted for each upper jaw velocity. Also, the force required to rupture the stem at 100, 300, and 500 mm min⁻¹ upper jaw velocities were measured. The test was carried out as a completely randomized design experiment in three replications. The results showed that velocity had a significant effect on the required force to thresh the paddy grain from spike, at probability levels of 5%. With an increase in velocity from 100 to 500 mm min⁻¹ the grain snapping force decreased from 4.77 to 1.09 N and the required force to rupture stem decreased from 33.43 to 8.41 N. Also, the normal stress acting on the stem due to grain snapping force and the ultimate stress of stem due to stem rupture force were calculated. According to the results obtained from this experiment, it can be concluded that the stem is not ruptured when the grains are being snapped from the spike. As illustrated in Fig. 5,. the maximum tensile force required to snap the grain from the stalk (4.77 N) was acquired at the velocity of 100 mm min⁻¹ Therefore, this force (4.77 N) was used to design various parts of the PHH.
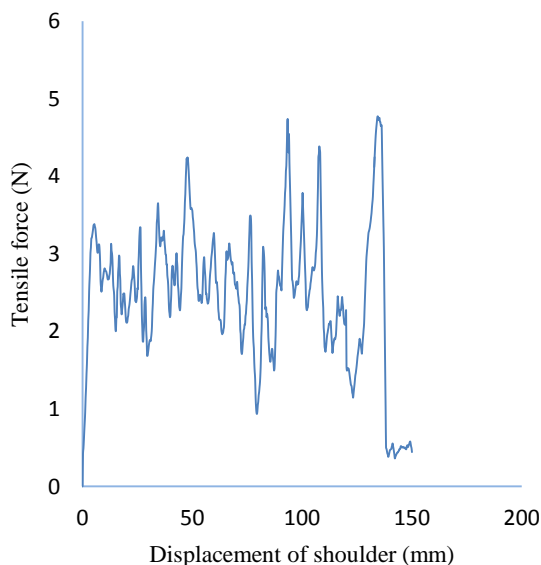

Fig. 5. The average of three replication of grain snapping force at a speed of 100 mm min⁻¹.

The OSS Analysis

Fig. 6(a) shows the stress distribution of the OSS in the most critical position (Just at the start of the second step). The maximum stress in the shoulder was 44.43 Mpa. Shoulder's critical point is shown in this figure. In order to have a closer look at the amount of stress and strain in the shoulder, some paths were defined on it. Fig.6 (b) shows the first path. This path starts from the

open end of the shoulder tooth and continues until the vertical shoulder wings.

Stress and strain curves of the first path are shown in Figs. 7(a) and (b), respectively. In these figures, the horizontal axis is the distance from beginning of the path. The amount of stress and strain have increased along the path. Maximum stress and strain in the shoulder tooth were 42.45 MPa and 0.00021, respectively.

The type of the mentioned stress was bending, which increases by the distance from the tip of the tooth. The strain diagram had similar trend as stress one. The second path was selected along the horizontal shoulder wing (Fig. 6c). This path starts from the open end of the shoulder and continues until the closed end of the shoulder. Figures 8(a) and (b) show the stress and strain curves for this path. The maximum values of stress and strain occured at the distance of 274 mm from the open end of shoulder which were 43.21 MPa and 0.00051, respectively.

The ISS Analysis

The purpose of this analysis was to determine the stress distribution in the bolts and part f of the ISS. Fig. 9 (a) shows the stress distribution in this shoulder at the most critical position (just at the start of the second step). Maximum stress in this shoulder was 66.68 MPa that occured at the shoulder bolt shank. The third path was defined for a closer examination of stress and strain at the top of the part f holes (Fig. 9b).

According to the stress and strain distribution diagram along the path 3, the maximum stress and strain values (Fig. 10) occured at the top of the hole centers of part f (Fig. 9 b). The maximum amount of stress and strain occur within 37.5 mm of the path beginning and were 39.83 MPa and 0.000155, respectively.

Due to the existence of two hole, the stress concentration occured. Therefore, the maximum stress and strain happened in the region near these two holes. To connect each shoulder to the axis, two bolts were used. The bolt shown in Fig. 9(c) is closer to the loading area, so it can withstand more stress. The fourth path was defined along the shank of this bolt (Fig. 9c). Stress and strain curves of this path are shown in the Figs. 11a and b, respectively. In these figures, the horizontal axis is the distance from the beginning of the path.

At the first 11.8 mm of the path, the bolt shank is in perfect contact with the inner surface of the shaft hole, so the stress and strain are low in this distance. At position of 5 mm (between the first nut and the IS) the strain and strain values are instantaneously increased. These values increase in the distance between the first and second nut (like as a beam). A sudden drop in stress and strain values in the range of 23.8 to 30.6 mm is due to contact between the inner surface of the second nut with the bolt shank. The maximum amount of stress and strain occured at the position 12 mm of the path beginning and were 65.45 MPa and 0.00161, respectively.
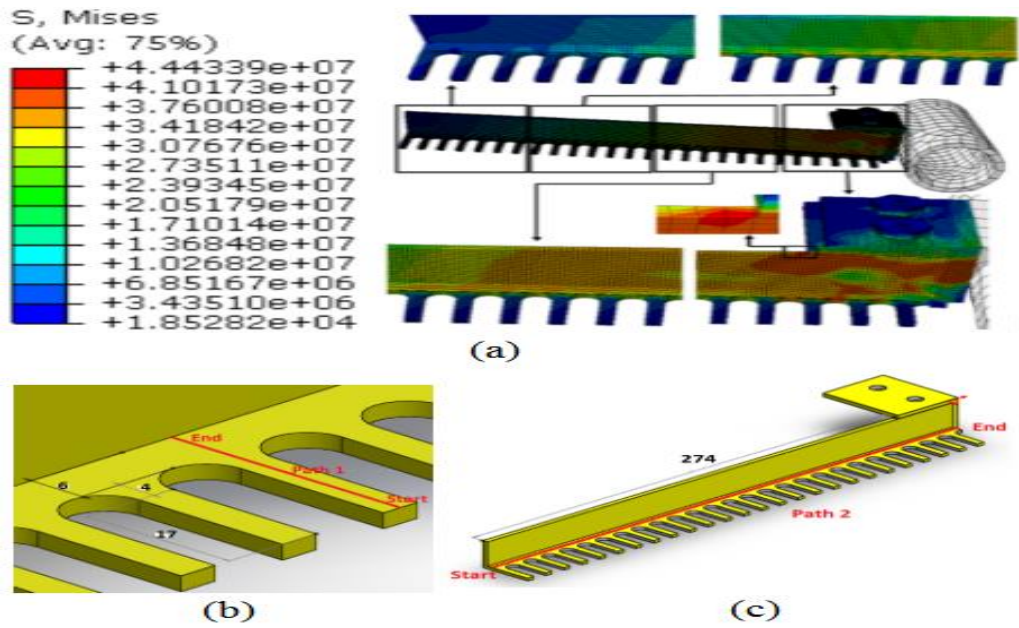
Fig. 6. (a) Stress distribution of OSS (Stress values are in Pascal); (b) Path 1; (c) Path 2 (Dimensions are in millimeter).
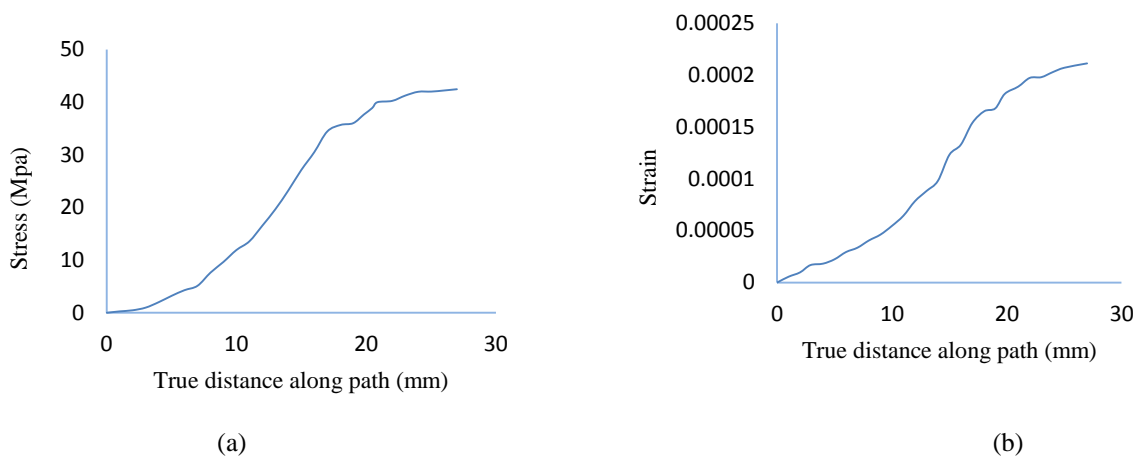

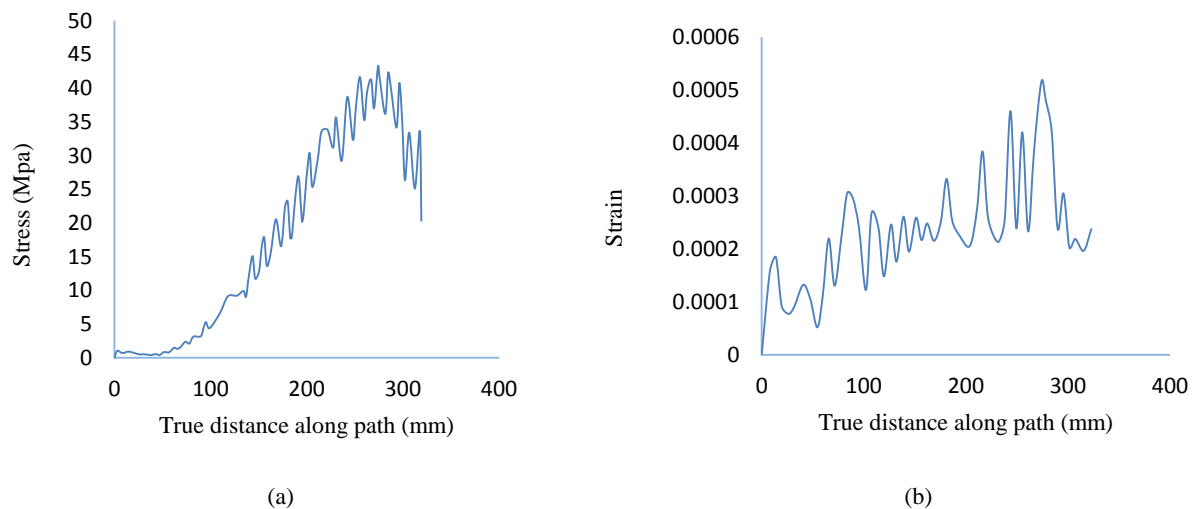**Fig. 7.** Stress and strain analysis through the Path 1; (a) Stress diagram; (b) Strain diagram.

Fig. 8. Stress and strain analysis through the Path 2; (a) Stress diagram; (b) Strain diagram.
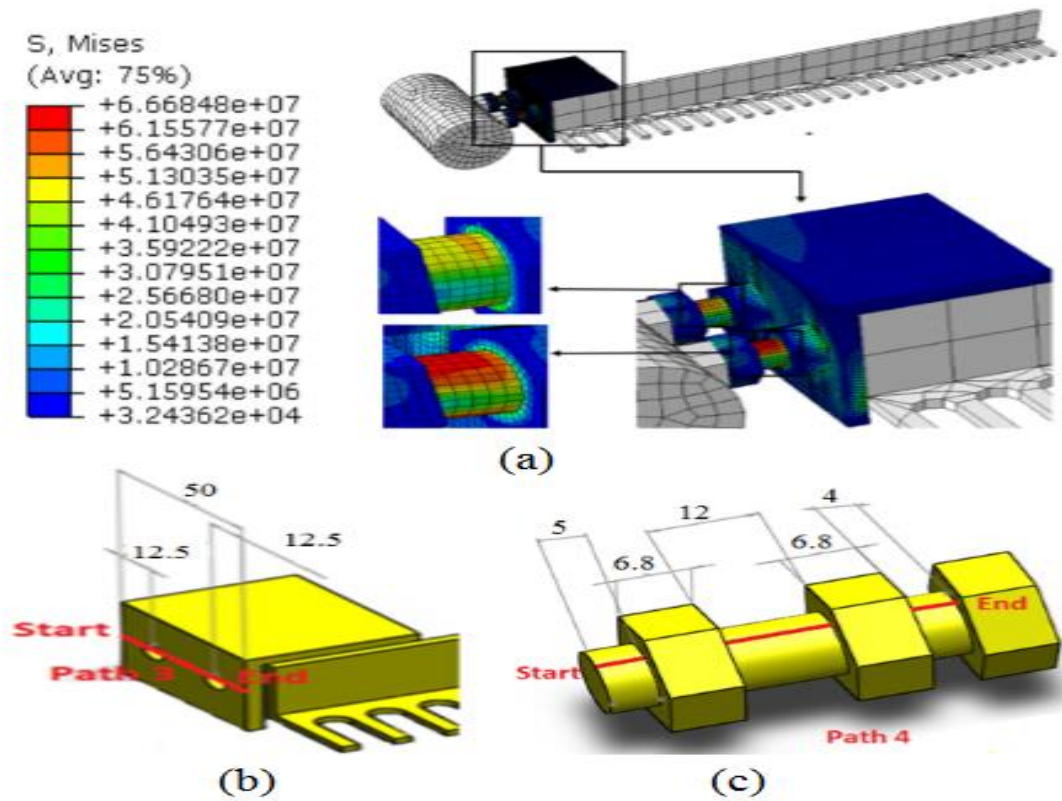
Fig. 9. (a) Stress distribution of ISS (Stress values are in Pascal); (b) Path 3; (c) Path 4 (Dimensions are in millimeter).
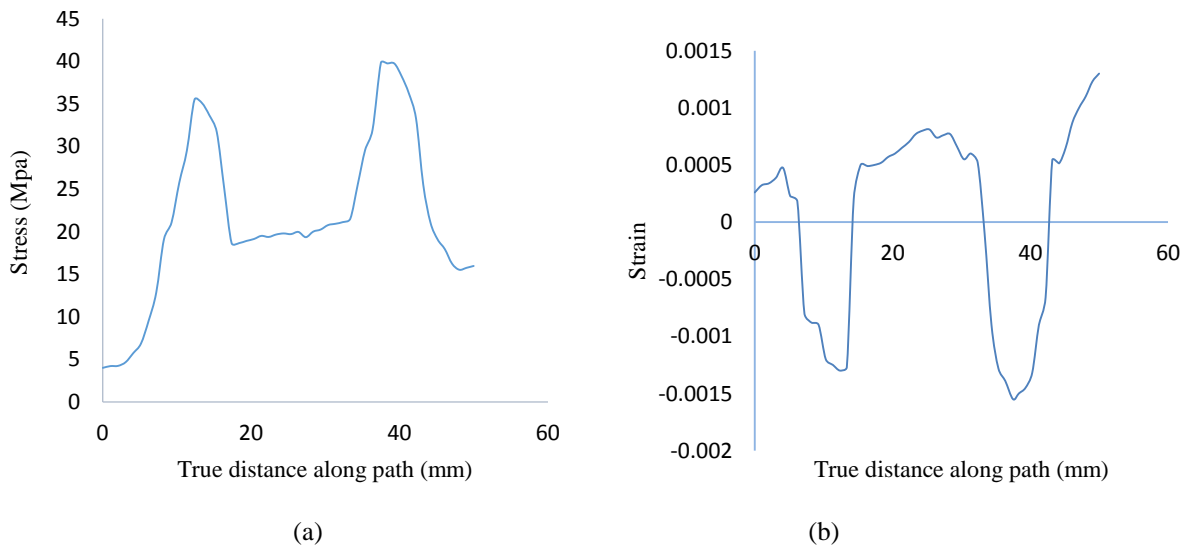

| (a) | (b) |

Fig. 10. Stress and strain analysis through the Path 3; (a) Stress diagram; (b) Strain diagram.

Fatigue Analysis

The factor of safety was used to provide a design margin over the theoretical design capacity to allow for uncertainty in the design process. The factor of safety for each component of OSS and ISS was calculated and results are shown in Table 3. As can be seen from this table, the fatigue FS for all components is less than yield factor of safety. Therefore, the fatigue in components will occur first. The stress-life method was used to predict the life in number of cycles to failure, N, for a specific level of loading. The predicted life for components OSS and ISS is in infinite-life region (Table 3). The selection of the appropriate FS to be used in the design of components is essentially a compromise between the associated additional cost and weight and the benefit of increased safety and/or reliability.
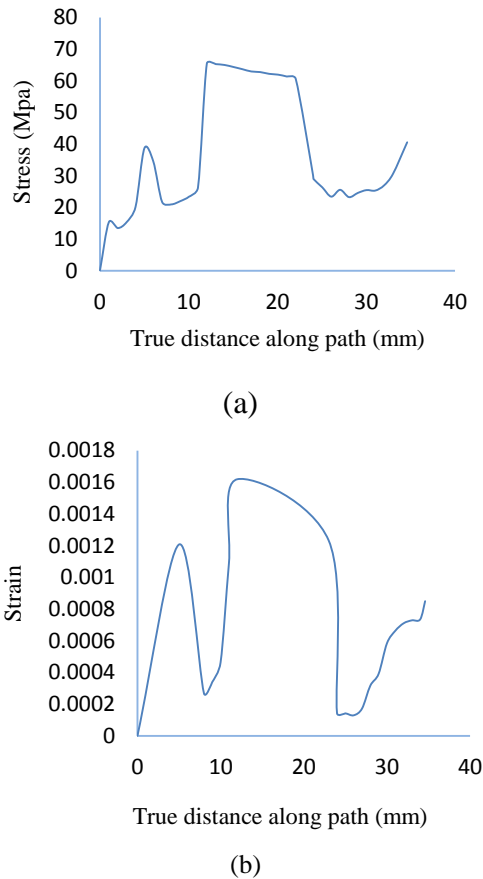
(a)

(b)

Fig. 11. Stress and strain analysis through the Path 4; (a) Stress diagram; (b) Strain diagram.

Table 3. Factor of safety and number of cycles to failure for of OSS and ISS components.

	Part 6	Bolts	Shoulder	Shoulder tooth
n_f	4.23	4.9	2.15	4.56
n_y	7.44	7.89	2.3	4.96
Number of cycles to failure	5.12×10^{13}	5.9×10^{13}	2.1×10^{13}	3.3×10^{13}

Model Validation

In the next step, an analytical method was exploited to verify the stress analysis of components. For this purpose, a number of sections were chosen through each path and the Von Misses stress was calculated for each section by Eq. (17) (Shigley, 2011; Li et al., 2008).

$$\sigma_{Von} = \{[((\sigma_x - \sigma_y)^2 + (\sigma_y - \sigma_z)^2 + (\sigma_z - \sigma_y)^2)/2] + 3(\tau_{xy}^2 + \tau_{yz}^2 + \tau_{xz}^2\}^{1/2}$$

(17)

In order to examine the overall validity of the FEM results, all the predicted values of stress were plotted

against the calculated values (Fig. 12). A regression line fitted to the data shows that the predicted stresses from analytical model lie within bounds of ± 7.89 % of the predicted values with a coefficient of determination to 0.98. Hence, it could be concluded that there is a good agreement between the analytical and FEM results.
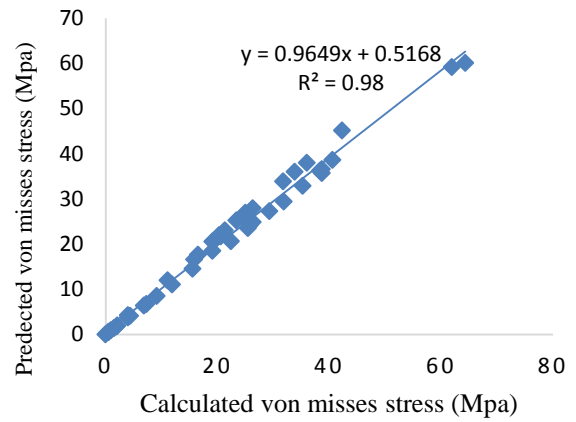

Fig. 12. Comparison of analytical and numerical Von Misses stress.

CONCLUSIONS

The stress and strain analysis of OSS and ISS of a new PHH were performed using FEM. The important findings of the current study are briefly reported as below.
1- The maximum amount of force applied to each tooth of shoulder was 4.29 N mm^{-1}.
2- The maximum stress in both of shoulders was found to be 44.43 MPa.
3- A regression line fitted to the data showed that the calculated stresses from analytical method lie within bounds of ± 7.89 % of the predicted values with a coefficient of determination to 0.98. Hence, it could be concluded that there is a good agreement between the analytical and FEM results.
4- The Fatigue analysis was conducted based on modified Goodman failure criteria and the results showed that the fatigue in components will occur first because fatigue FS for all components is less than yield FS. Also, the modified Goodman failure criteria was used to estimate the OSS and ISS components life (N). The predicted life for all components were in infinite-life region (N$\geq 10^6$ cycle), thus the components have an infinite-life.

ACKNOWLEDGEMENT

REFERENCES

Abdulkarim, K., Abdulrahman, K., Ahmed, I., Abdulkareem, S., ADEBISI, J., & Harmanto, D. (2017). Finite element analysis of mini combined harvester chassis and hitch. *Journal of Production Engineering*, 20, 48-54.

Azimi Nejadian, H. (2016). *Design and fabrication of a head for paddy harvesting machine*. (Master's thesis, University of Tarbiat Modares, Tehran, Iran). (In Persian).

Azimi Nejadian, H., Tavakoli Hashjin, T., Ghobadian, B. & Hoseini, S. S., (2016). Measurement requirement force to separate the grain paddy for design of rice harvesting head. *Iranian Journal of Biosystems Engineering,* 47(2), 337-343. (In Persian).

Azimi-Nejadian, H., Karparvarfard, S. H., Naderi-Boldaji, M., & Rahmanian-Koushkaki, H. (2019). Combined finite element and statistical models for predicting force components on a cylindrical mouldboard plough. *Biosystems Engineering*, 186, 168-181.

Beni, Y. T., Vahdati, A. R., & Abadyan, M. (2013). Using ALE-FEM to simulate the instability of beam-type nano-actuator in the presence of electrostatic field and dispersion forces. *Iranian Journal of Science and Technology. Transactions of Mechanical Engineering*, 37(M1), 1-9.

Bursi, O. S., & Jaspart, J. P. (1998). Basic issues in the finite element simulation of extended end plate connections. *Computers & Structures*, 69(3), 361-382.

Chandrajith, U. G., Gunathilake, D. M. C. C., Bandara, B. D. M. P., & Swarnasiri, D. P. C. (2016). Effects of combine harvesting on head rice yield and chaff content of long and short grain paddy harvest in Sri Lanka. *Procedia Food Science*, 6, 242-245.

Denguir, L. A., Outeiro, J. C., Rech, J., Fromentin, G., Vignal, V., & Besnard, R. (2017). Friction model for tool/work material contact applied to surface integrity prediction in orthogonal cutting simulation. *Procedia CIRP*, 58, 578-583.

Elsawaf, S. A., & Hassan, M. M. (2018). Behaviour of structural sub-assemblies of steel beams with openings in fire conditions. *Journal of Constructional Steel Research*, 148, 627-638.

Elsoragaby, S., Yahya, A., Mahadi, M. R., Nawi, N. M., & Mairghany, M. (2019). Comparative field performances between conventional combine and mid-size combine in wetland rice cultivation. *Heliyon*, 5(4), 1-25.

Fadaei, A., & Mokhtari, H. (2015). Finite element modeling and experimental study of residual stresses in repair butt weld of ST-37 plates. *Iranian Journal of Science and Technology Transactions of Mechanical Engineering*, 39, 291-307.

Fu, L., Peng, J., Nan, Q., He, D., Yang, Y., & Cui, Y. (2016). Simulation of vibration harvesting mechanism for sea buckthorn. *Engineering in Agriculture, Environment and Food*, 9(1), 101-108.

Fu, Y. B., & Chui, C. K. (2014). Modelling and simulation of porcine liver tissue indentation using finite element method and uniaxial stress–strain data. *Journal of Biomechanics*, 47(10), 2430-2435.

Gao, S. (2019). Nonlinear finite element failure analysis of bolted steel-concrete composite frame under column-loss. *Journal of Constructional Steel Research*, 155, 62-76.

Harewood, F. J., & McHugh, P. E. (2007). Comparison of the implicit and explicit finite element methods using crystal plasticity. *Computational Materials Science*, 39(2), 481-494.

Heintze, S. D., Monreal, D., Reinhardt, M., Eser, A., Peschke, A., Reinshagen, J., & Rousson, V. (2018). Fatigue resistance of all-ceramic fixed partial dentures–Fatigue tests and finite element analysis. *Dental Materials*, 34(3), 494-507.

Horgan, F. G., Ramal, A. F., Bernal, C. C., Villegas, J. M., Stuart, A. M., & Almazan, M. L. (2016). Applying ecological engineering for sustainable and resilient rice production systems. *Procedia Food Science*, 6, 7-15.

Jahanbakhshi, A., & Heidarbeigi, K. (2019). Simulation and mechanical stress analysis of the lower link arm of a tractor using finite element method. *Journal of Failure Analysis and Prevention,* 19(6), 1666-1672.

Jahanbakhshi, A., Ghamari, B., & Heidarbeigi, K. (2017). Assessing acoustic emission in 1055I John Deere combine harvester using statistical and artificial intelligence methods. *International Journal of Vehicle Noise and Vibration,* 13(2), 105-117.

Jain, R., Pal, S. K., & Singh, S. B. (2018). Finite element simulation of pin shape influence on material flow, forces in friction stir welding. *The International Journal of Advanced Manufacturing Technology*, 94(5-8), 1781-1797.

Khanali, M., Jafari, A., Mobli, H., & Rajabipour, A. (2010). Analysis and design optimization of a frontal combine harvester axle using finite element and experimental methods. *Journal of Food, Agriculture & Environment*, 8(2), 359-364.

Kim, J., Yoon, J. C., & Kang, B. S. (2007). Finite element analysis and modeling of structure with bolted joints. *Applied Mathematical Modelling*, 31(5), 895-911.

Li, H., Zhao, G., & He, L. (2008). Finite element method based simulation of stress–strain field in the quenching process. *Materials Science and Engineering: A*, 478(1-2), 276-290.

McCarthy, M. A., McCarthy, C. T., Lawlor, V. P., & Stanley, W. F. (2005). Three-dimensional finite element analysis of single-bolt, single-lap composite bolted joints: Part I—model development and validation. *Composite Structures*, 71(2), 140-158.

Motevali, A., Hashemi, S. J., & Tabatabaeekoloor, R. (2019). Environmental footprint study of white rice production chain-case study: Northern of Iran. *Journal of Environmental Management*, 241, 305-318.

Muntakim, A., Siddiquee, M., & Udagepola, K. (2016). Finite element simulation of the effect of loading rate on the stress-strain behaviour of Albany sand. *Journal of the National Science Foundation of Sri Lanka*, 44(2), 203-209.

Reid, J. D., & Hiser, N. R. (2005). Detailed modeling of bolted joints with slippage. *Finite Elements in Analysis and Design*, 41(6), 547-562.

Seyedabadi, E. (2015). Finite element analysis of lift arm of a MF-285 tractor three-point hitch. *Journal of Failure Analysis and Prevention, 15(5)*, 737-743.

Shahani, A. R., Shakeri, I., & Kashani, H. M. (2015). Fatigue life estimation of bolts in flanges of a reinforced cylindrical shell. *Modares Mechanical Engineering*, 14(13), 201-208. (In Persian).

Shaw, M. C., & Cookson, J. O. (2005). *Metal cutting principles* (Vol. 2). New York: Oxford University Press.

Shigley, J. E. (2011). *Shigley's mechanical engineering design*. New York: Tata McGraw-Hill Education.

Soltani, P., & Mirhosseini, R. T. (2013). Study of non-linear dynamic behavior of structures with steel shear wall under the near fault earthquakes. *Journal of Civil Engineering and Urbanism*, 3(6), 372-379.

Tanlak, N., Sonmez, F. O., & Talay, E. (2011). Detailed and simplified models of bolted joints under impact loading. *The Journal of Strain Analysis for Engineering Design*, 46(3), 213-225.

Ucgul, M., Saunders, C., & Fielke, J. M. (2018). Comparison of the discrete element and finite element methods to model the interaction of soil and tool cutting edge. *Biosystems Engineering*, 169, 199-208.

Umbrello, D. (2008). Finite element simulation of conventional and high speed machining of Ti6Al4V alloy. *Journal of Materials Processing Technology*, 196(1-3), 79-87.

Ushio, Y., Saruwatari, T., & Nagano, Y. (2019). Elastoplastic FEM analysis of earthquake response for the field-bolt joints of a tower-crane mast. *Advances in Computational Design*, 4(1), 53-72.

Yorgun, C., Dalcı, S., & Altay, G. A. (2004). Finite element modeling of bolted steel connections designed by double channel. *Computers & structures*, 82(29-30), 2563-2571.

Zhao, Z., Huang, H., Yin, J., & Yang, S. X. (2018). Dynamic analysis and reliability design of round baler feeding device for rice straw harvest. *Biosystems Engineering*, 174, 10-19.

مقاله علمی- پژوهشی

واکاوی مکانیکی سامانه جدا کننده دانه از خوشه یک هد جدید برداشت دانه‌های شلتوک

هادی عظیمی نژادیان*[1]، تیمور توکلی هشجین[2]، محمد امین نعمت اللهی[1]، سید حسین کارپرورفرد[1]

[1]گروه مهندسی مکانیک بیوسیستم، دانشگاه شیراز، شیراز، ج. ا. ایران

[2]گروه مهندسی مکانیک بیوسیستم، دانشگاه تربیت مدرس، تهران، ج. ا. ایران

*نویسنده مسئول

چکیده- در این مقاله تحلیل تنش و کرنش شانه محور بیرونی و شانه محور درونی هد برداشت جدید برنج با استفاده از روش المان محدود ارائه می‌شود. این هد برداشت شامل سامانه جدا کننده دانه از ساقه بوده که هریک از شانه‌های محورهای بیرونی و درونی عضوی از این سامانه می‌باشند. از نرم‌افزار اباکوس با حلگر صریح دینامیکی برای انجام واکاوی، و از بلوک‌های هشت گره‌ای و المان‌های تتراهدرال به منظور المان‌بندی قطعات استفاده شد. پس از اتمام شبیه‌سازی، نمودارهای تنش و کرنش قطعات رسم شده و مقادیر بیشینه آن‌ها در هر یک از قطعات تعیین شد. از روش تحلیلی به منظور صحت سنجی نتایج حاصل از شبیه‌سازی و همچنین محاسبه ضریب اطمینان و تعیین عمر هر یک از قطعات استفاده شد. حداکثر میزان نیروی اعمال شده بر روی هر دندانه شانه ۴/۲۹ نیوتن بر میلیمتر بود. حداکثر تنش در هر دو شانه ۴۴/۴۳ مگاپاسکال بدست آمد. نتایج نشان داد ضریب اطمینان خستگی تمام قطعات از ضریب اطمینان تسلیم آن‌ها کمتر است. بنابراین قطعات زودتر دچار خستگی می‌شوند. عمر محاسبه شده برای هر یک از قطعات بیشتر از 10^6 بود. بنابراین قطعات (شانه محور بیرونی و شانه محور درونی) در محدوده عمر نامحدود قرار دارند. خط رگرسیون با ضریب تبیین ۰/۹۸ بر داده‌ها انطباق داده شد و همچنین اختلاف بین داده‌های پیش‌بینی شده از روش المان محدود و محاسبه شده با روش تحلیلی در محدوده ۷/۸۹± بود. بنابراین می‌توان نتیجه گرفت که انطباق قابل قبولی بین داده‌های پیش‌بینی شده و محاسبه شده، وجود دارد.